Supplement of Geosci. Model Dev., 16, 5949–5977, 2023
https://doi.org/10.5194/gmd-16-5949-2023-supplement

Geoscientific Model Development
Open Access
EGU

Supplement of

A Regional multi-Air Pollutant Assimilation System (RAPAS v1.0) for emission estimates: system development and application

Shuzhuang Feng et al.

Correspondence to: Fei Jiang (jiangf@nju.edu.cn)

Text S1

Figure S3 shows the analysis increments (assimilation minus control) of the 6 species averaged over all initializations. It could be found that the impact of 3DVAR is not only concentrated around the measurement sites, but also transported to downwind areas as discussed in Feng et al. (2018). The longer a species lives, the farther the assimilation benefits are transmitted (e.g., CO). The positive (negative) increments indicate underestimated (overestimated) emissions in local or upwind areas. Specifically, the positive increments of CO and PMC are generally distributed nationwide, especially in the northern part of China, indicating that the emissions of CO and PMC over the mainland China were estimated, which may be related to the underestimated residential sources (e.g., coal heating) (Zhi et al., 2017) and local dust caused by higher wind speeds, respectively. For SO_2, NO_2 and $PM_{2.5}$, the negative increments are mainly located in the North China Plain (NCP), the Yangtze River Delta (YRD), and the Sichuan Basin (SCB), as well as Central China, and the significant positive increments mainly correspond with resource-abundant northern regions (e.g., Northeast China, Northwest China, etc.). The increments of $PM_{2.5}$ are related not only to inaccurate emissions but also to the concentration biases of its precursor, which can affect the biases of $PM_{2.5}$ in downwind areas to some extent. The increments of O_3 are negatively correlated with those of NO_2 in terms of their spatial distribution because of strong NO-titration during the winter (Huang et al., 2020; Shi and Brasseur, 2020).

Text S2

In the EnKF-based inverse estimation scheme, the uncertainty is represented by the spread of the ensemble samples (Tang et al., 2013). The posterior and prior uncertainties are the standard deviations of the prior and posterior perturbations of $\boldsymbol{X_i^b}$ and $\boldsymbol{X_i^a}$. $\boldsymbol{X_i^b}$ was perturbed from the prior emissions $\boldsymbol{X_0^b}$ by adding a randomly perturbed item of $\boldsymbol{\delta X_i^b}$, which was drawn from Gaussian distributions with a mean of zero and the standard deviation of the prior emission uncertainty in each grid. After constrained using observations, the perturbed emissions of $\boldsymbol{X_i^b}$ is changed to $\boldsymbol{X_i^a}$ according to Eq. 2 ~ 5.

$$\boldsymbol{X_i^b} = \boldsymbol{X_0^b} + \boldsymbol{\delta X_i^b} \ , i = 1, 2, \dots , N \tag{1}$$

$$\boldsymbol{X_i^a} = \boldsymbol{X^a} + (\boldsymbol{X_i^b} - \boldsymbol{X^b}) - \widetilde{\boldsymbol{K}}\boldsymbol{H}(\boldsymbol{X_i^b} - \boldsymbol{X^b}) \tag{2}$$

$$\widetilde{\boldsymbol{K}} = \left(1 + \sqrt{\boldsymbol{R}/(\boldsymbol{H}\boldsymbol{P^b}\boldsymbol{H}^T + \boldsymbol{R})}\right)^{-1}\mathbf{K} \tag{3}$$

$$\mathbf{K} = \boldsymbol{P^b}\boldsymbol{H}^T(\boldsymbol{H}\boldsymbol{P^b}\boldsymbol{H}^T + \boldsymbol{R})^{-1} \tag{4}$$

$$\boldsymbol{P^b} = \frac{1}{N-1}\sum_{i=1}^{N}(\boldsymbol{X_i^b} - \overline{\boldsymbol{X}}^{\boldsymbol{b}})\,(\boldsymbol{X_i^b} - \overline{\boldsymbol{X}}^{\boldsymbol{b}})^T \tag{5}$$

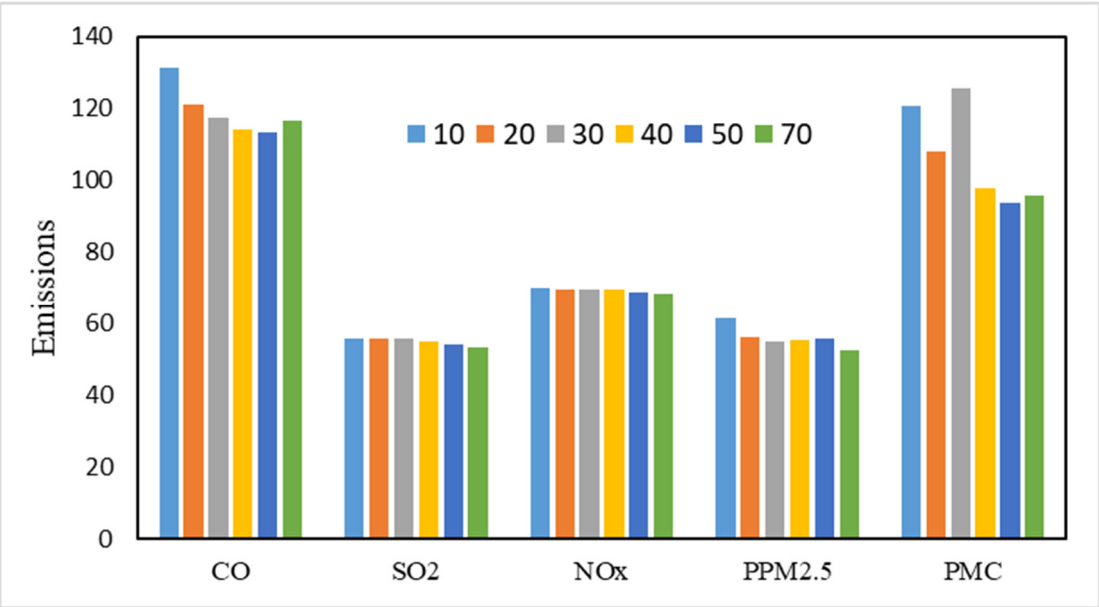

Figure S1 Comparison of emissions of different species inferred by selecting different ensemble numbers. CO unit:10 Gg; others units: Gg.

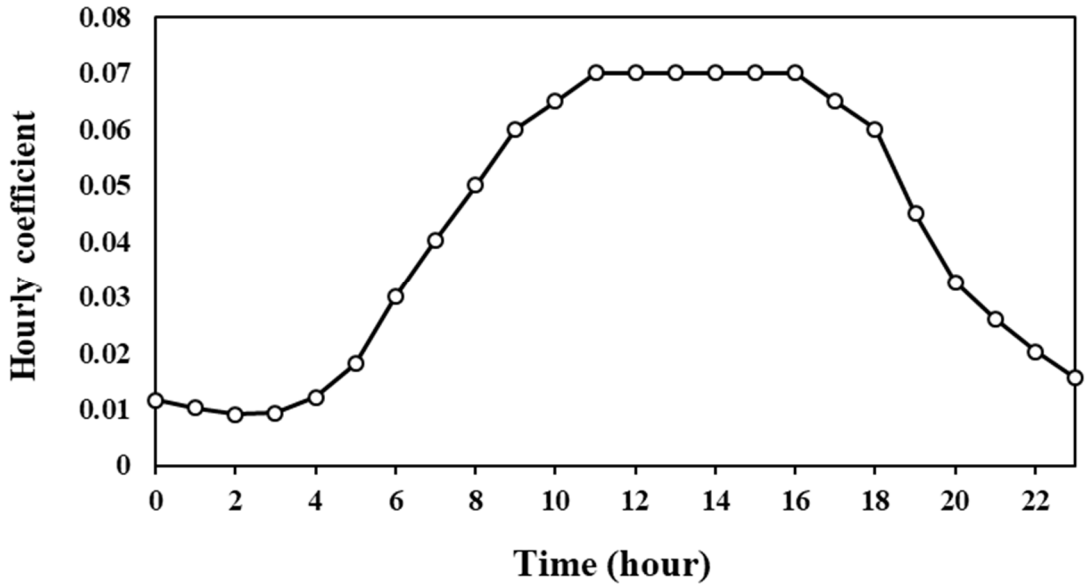

Figure S2. Hourly emission variabilities.

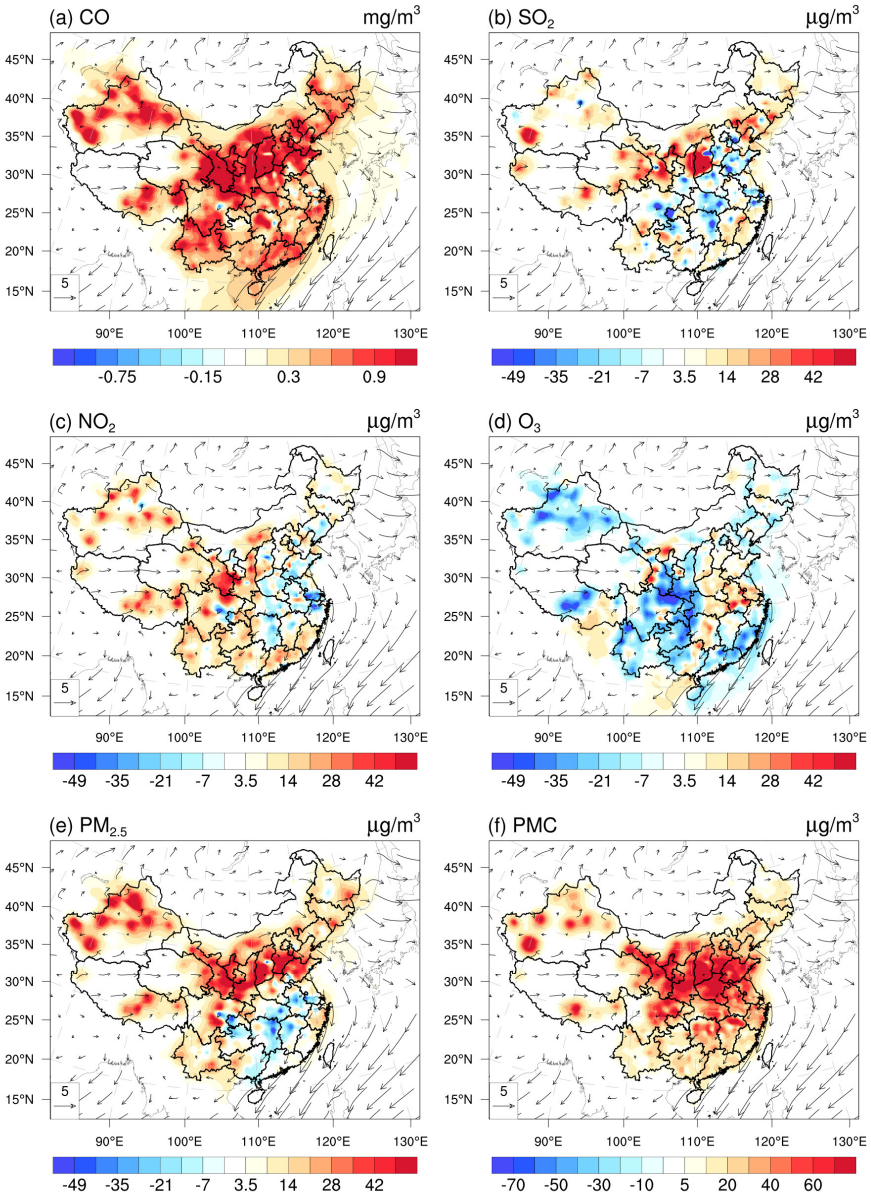

Figure S3. Mean differences of the background and analysis fields of (a) CO, (b) SO_2, (C) NO_2, (d) O_3, (e) $PM_{2.5}$ and (f) PMC at the lowest model level (analysis fields minus background fields). All data are averaged using the fields at 0000, 0600, 1200, and 1800 UTC during the period of 27 to 01 December, 2016.

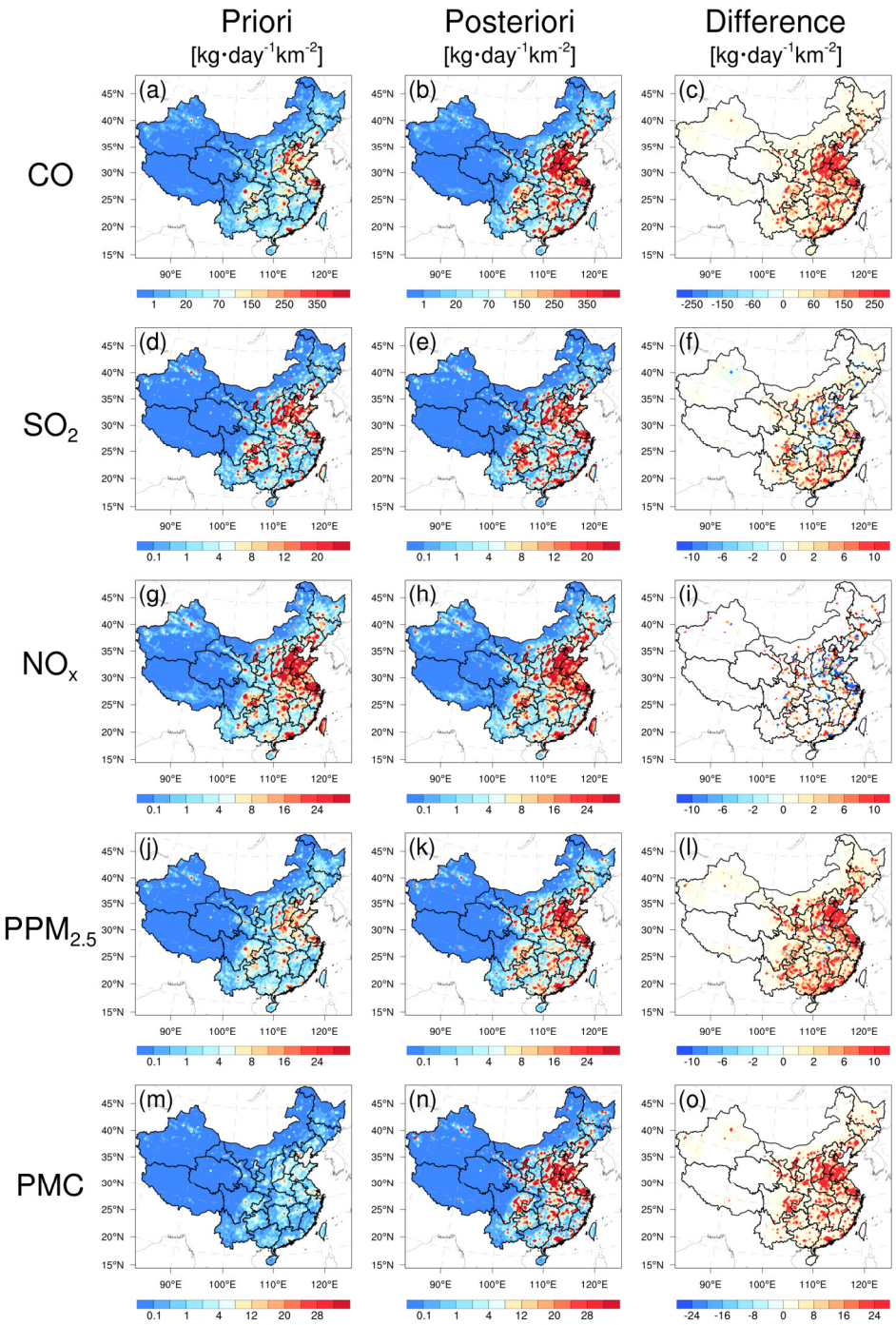

Figure S4. Spatial distribution of the time-averaged prior emissions (left column, MEIC 2016), posterior emissions (middle column), and differences (right column, posterior minus prior) in July 2016.

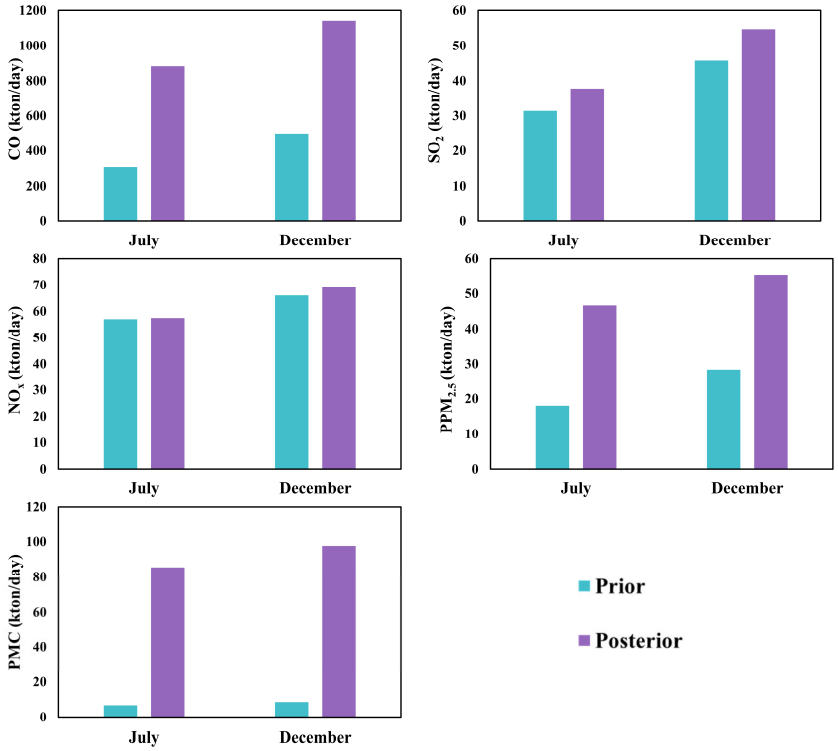

Figure S5. The prior and posterior emissions (kton/day) in July and December 2016 over the mainland China.

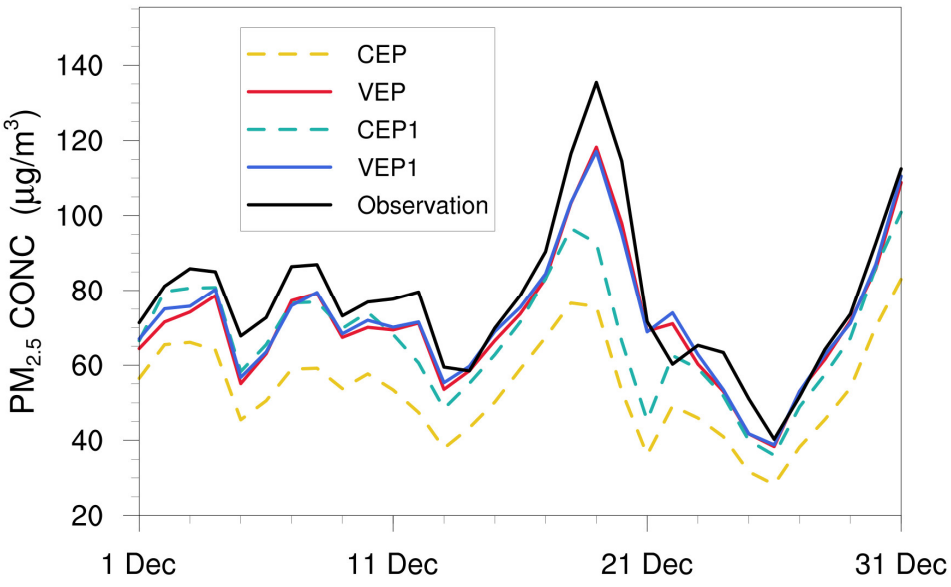

Figure S6. Time series of the daily $PM_{2.5}$ concentrations (CONC, μg m^{-3}) averaged over the whole domain obtained from the observations and simulations. CEP1 and VEP1 represent simulations using prior emissions taken from MEIC 2012 and posterior emissions inferred by EMS1 experiment, respectively.

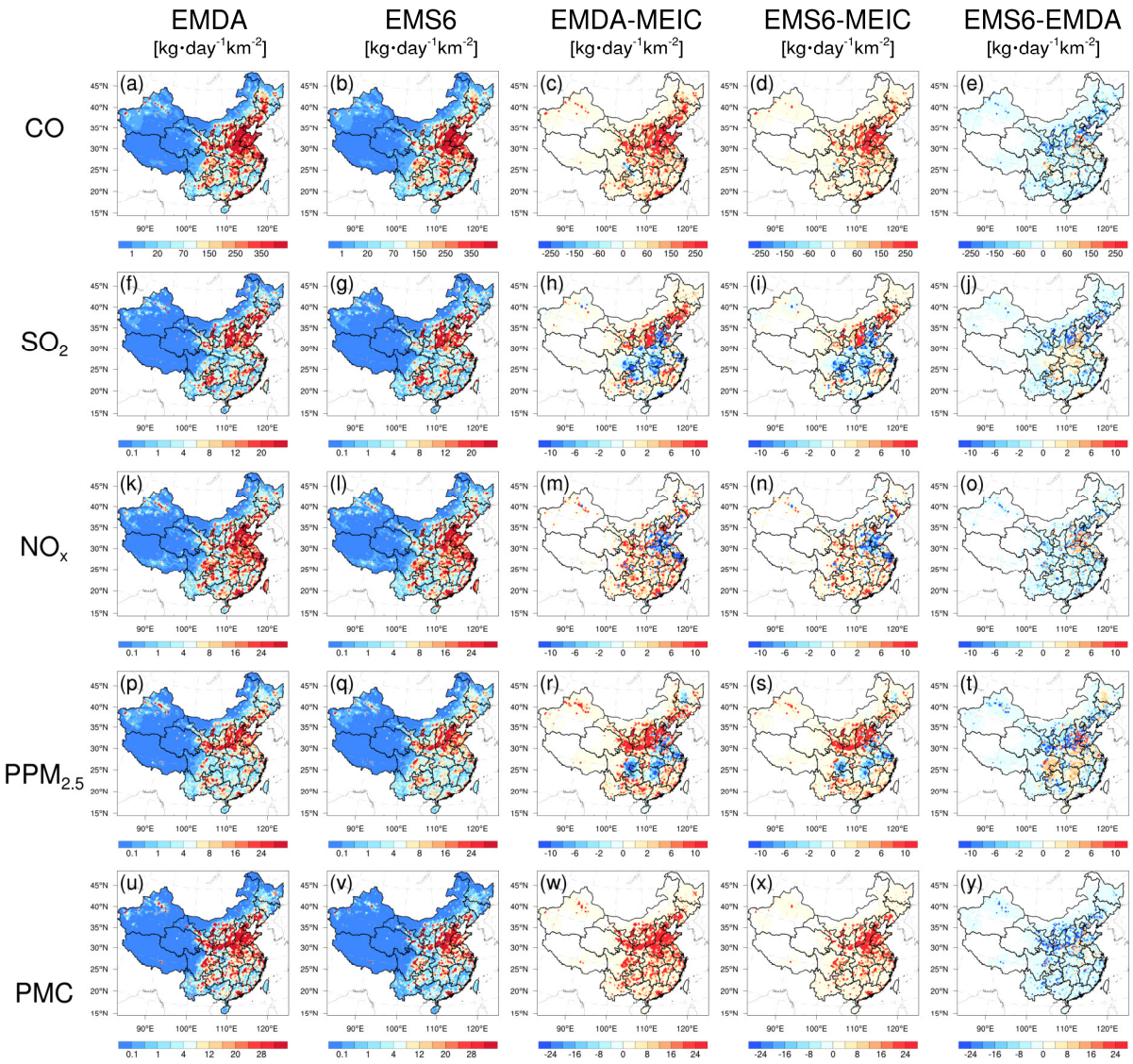

Figure S7. Spatial distribution of the time-averaged posterior emissions of EMDA and EMS6, and differences among prior emissions (MEIC) and posterior emissions of EMDA and EMS6.

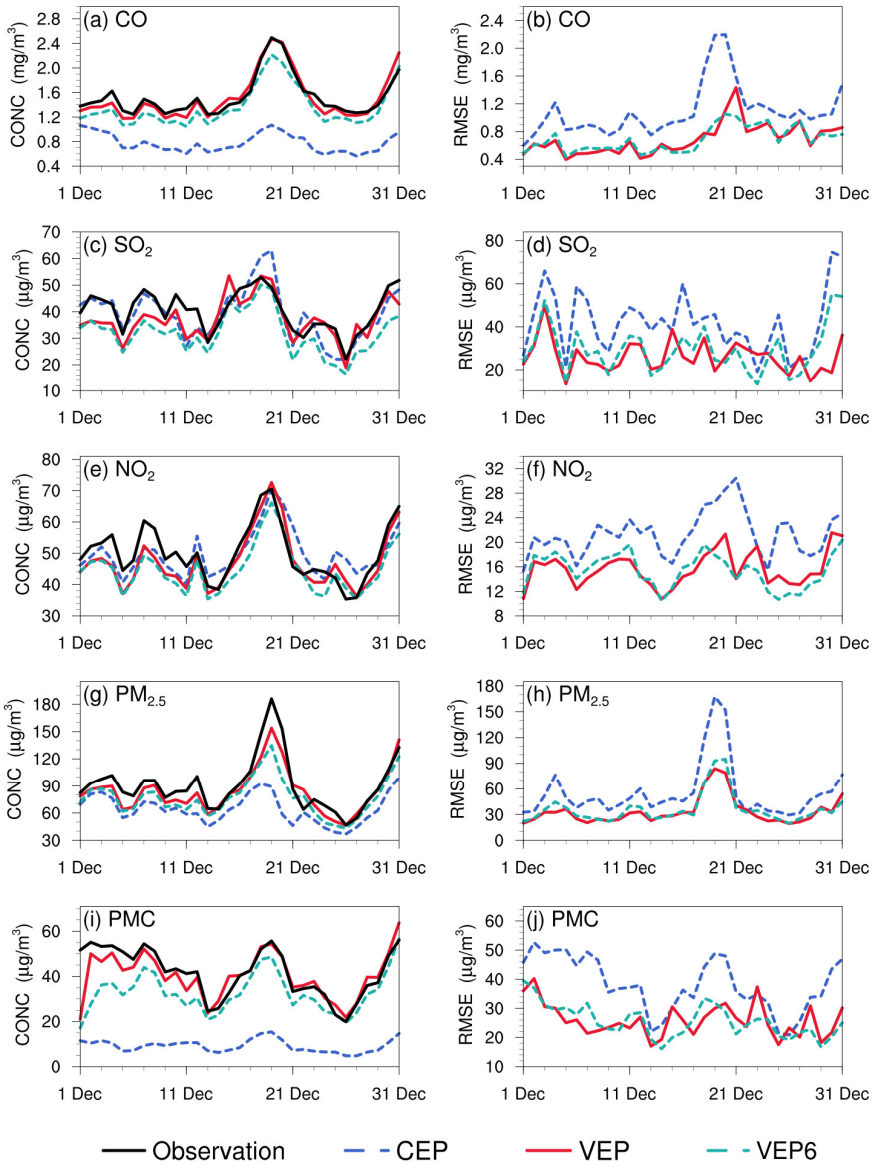

Figure S8. Time series of the daily concentrations (CONC, left, μg m^{-3}) and root mean square error (RMSE, right, μg m^{-3}) obtained from CEP, VEP, and VEP6. The simulations were verified against the independent sites.

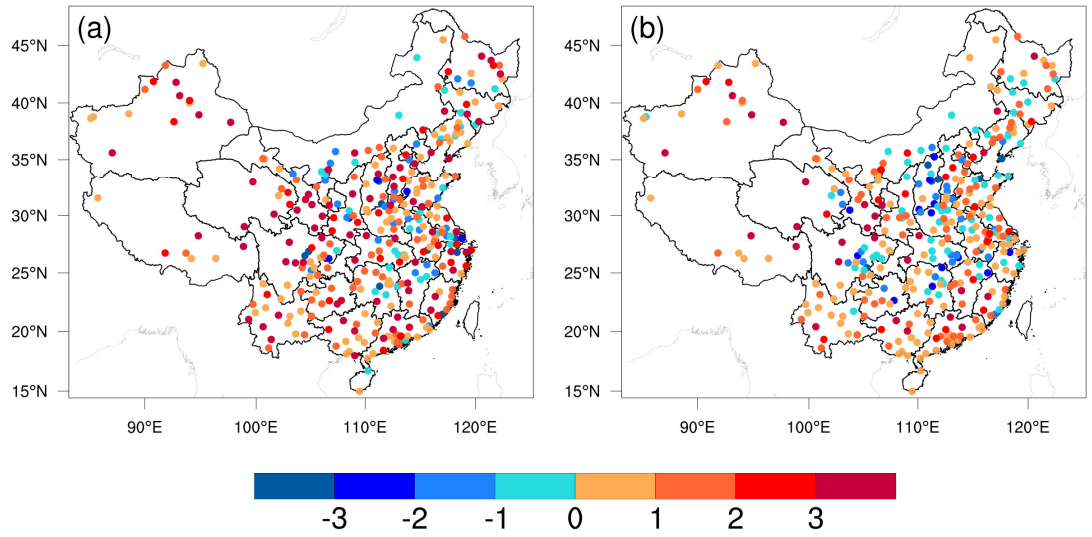

Figure S9. Changes of the (a) BIAS (μg m^{-3}) and (b) RMSE (μg m^{-3}) of the simulated NO_2 between VEP and VEP6 experiments.

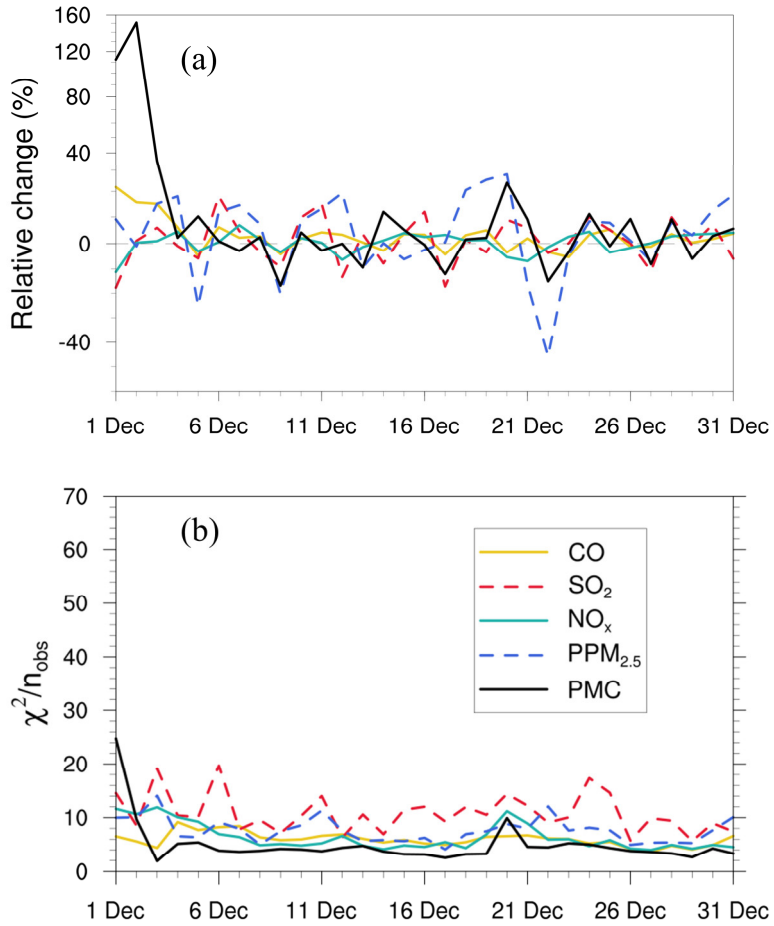

Figure S10. Relative changes (a) in a posteriori emission estimates of CO, SO_2, NO_x, $PPM_{2.5}$ and PMC, and χ^2 statistics (b) of these state vectors in EMS6 experiment.

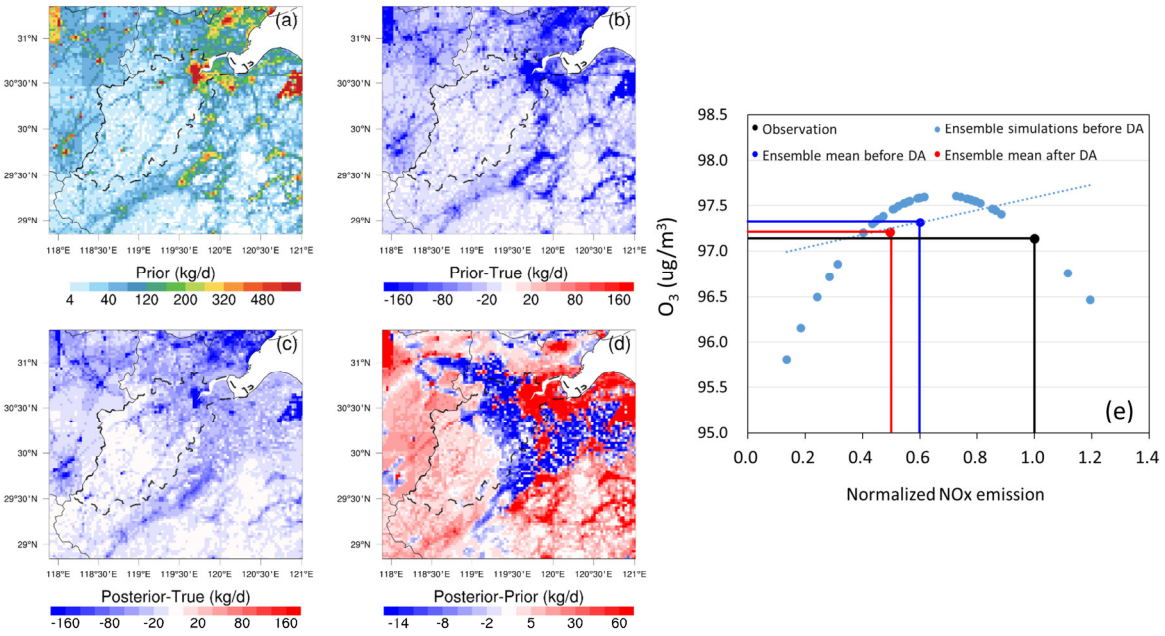

Figure S11. Spatial distribution of (a-d) the prior, posterior, 'true' emissions, and their differences (kg/d), as well as (e) the changes in NO_x emissions and simulated O_3 concentrations before and after assimilating O_3 observation. The "true" emissions were reduced by 40% to represent the a priori emissions in the first OSSE experiment, and a representative grid with a negative NO_x adjustment were selected to demonstrate the limitations of assimilating O_3 in NO_x adjustment in the second OSSE experiment.

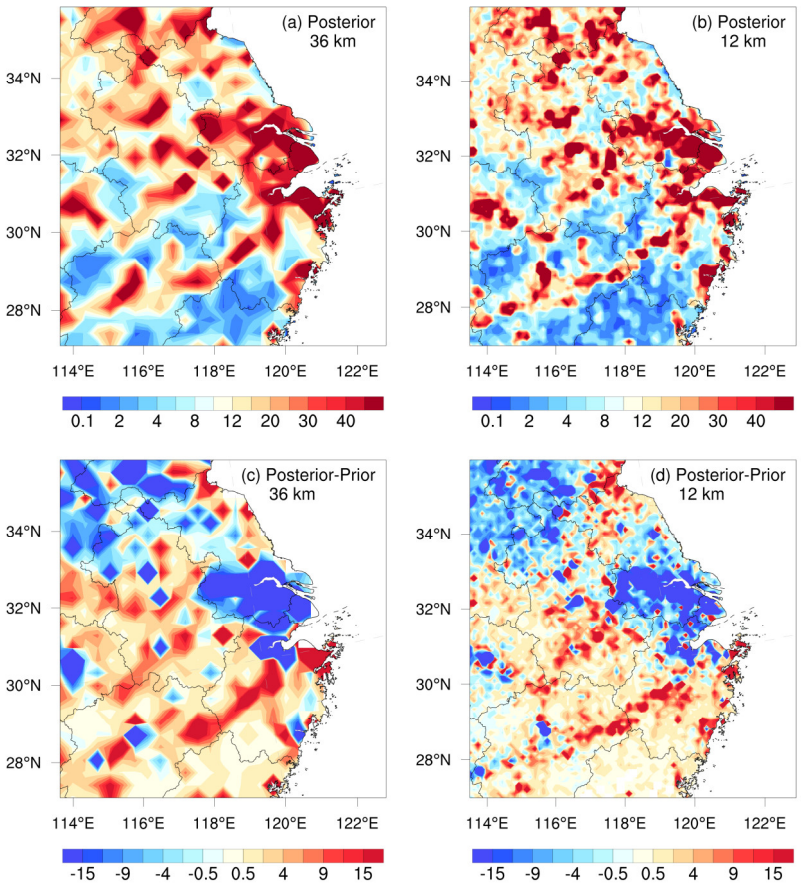

Figure S12. Spatial distribution of the time-averaged posterior NOx emissions (kg day^{-1}km^{-2}) and differences between posterior and prior NOx emissions (posterior minus prior) at 36 and 12 km resolutions.

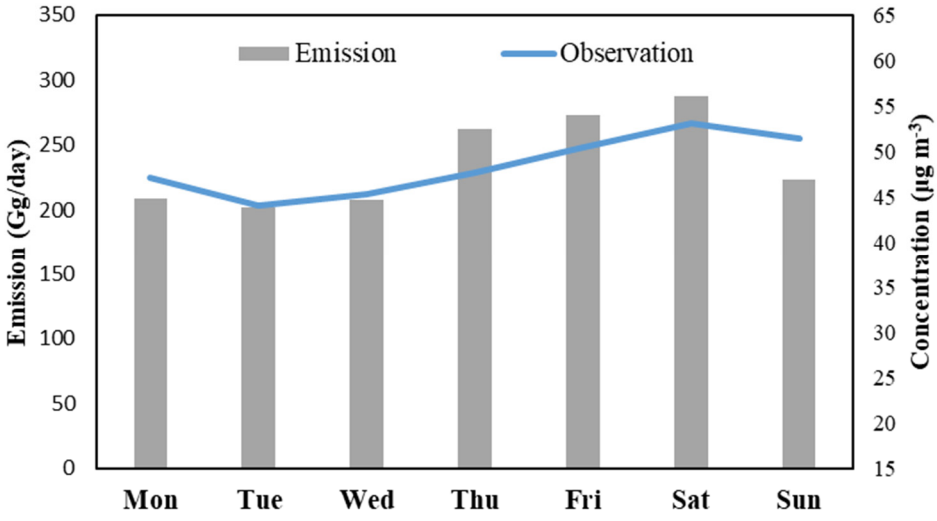

Figure S13. Weekly variation in posterior NOx emission and NO_2 observation.

Table S1. Estimation of posterior emissions (kton/day) and relative changes (%) compared to prior emissions in each province and the mainland China.

Region	CO		SO_2		NO_X		$PPM_{2.5}$		PMC	
	Post.	Diff.	Post.	Diff.	Post.	Diff.	Post.	Diff.	Post.	Diff.
Mainland	1141.9	129.4	54.7	19.7	69.4	5.1	55.4	95.4	97.6	1044.8
Shanghai	4.75	12.5	0.25	-59.5	0.74	-44.0	0.11	-40.8	0.22	249.1
Jiangsu	37.27	30.9	1.10	-23.9	2.90	-38.6	0.96	-34.3	2.46	529.6
Zhejiang	20.15	80.3	0.59	-30.0	2.68	1.9	0.86	77.9	2.15	876.9
Anhui	32.88	69.6	0.79	21.3	2.79	1.5	1.28	-3.0	2.50	495.6
Shandong	93.11	115.9	3.33	-17.5	4.26	-32.7	3.07	19.3	6.11	742.6
Beijing	6.34	108.4	0.06	-15.7	0.35	22.0	0.23	80.7	0.19	544.3
Tianjin	13.40	372.2	0.11	-33.6	0.59	53.3	0.23	73.7	0.35	933.0
Hebei	125.45	158.4	3.47	10.9	5.49	1.1	6.00	176.3	8.23	1176.7
Shanxi	82.17	210.9	9.93	86.9	2.88	-15.4	5.66	236.1	7.20	1274.8
Neimenggu	59.12	231.2	5.48	135.8	3.92	29.0	2.73	163.7	7.11	2144.3
Henan	69.99	120.2	1.14	-39.6	3.09	-22.7	3.05	66.6	6.26	1008.4
Hunan	40.59	56.8	1.52	-40.3	2.36	-5.2	0.69	-52.9	2.98	481.5
Hubei	38.80	73.1	0.57	-76.5	2.27	-1.9	1.17	-12.1	2.32	498.7
Jiangxi	28.71	112.3	1.63	83.0	1.78	19.0	1.52	110.3	2.65	777.5
Guangdong	52.97	175.3	1.19	-32.7	4.66	31.1	1.91	89.4	2.65	565.6
Guangxi	24.81	120.8	1.18	-1.5	2.30	52.2	1.70	103.6	1.75	512.5
Fujian	12.22	113.8	0.81	60.3	1.91	57.8	0.75	99.0	1.35	904.3
Hainan	1.94	20.5	0.14	-10.0	0.31	6.6	0.09	-17.0	0.07	106.9
Liaoning	49.69	175.2	4.04	178.8	2.71	-5.9	1.99	94.7	3.93	1377.3
Heilongjiang	38.64	90.2	1.10	25.7	1.82	-2.6	1.40	25.6	0.99	345.6
Jilin	35.61	176.2	3.36	376.2	2.46	69.2	1.72	132.1	0.87	437.8
Shaanxi	49.30	212.9	1.62	-9.5	2.40	37.7	3.64	294.2	7.25	2750.2
Gansu	49.41	423.7	1.51	118.6	1.97	100.1	3.27	521.4	9.64	8264.2
Xinjiang	39.94	383.4	1.48	21.0	2.69	48.2	4.29	720.3	2.69	1523.5
Qinghai	7.15	236.0	0.31	128.4	0.36	23.4	0.36	147.3	1.27	2948.9
Ningxia	14.34	523.8	1.96	129.6	1.06	16.6	1.14	478.6	2.95	3603.5
Sichuan	36.88	46.3	1.11	-43.2	3.20	7.4	1.66	8.1	4.54	1073.8
Chongqing	9.75	24.2	0.48	-69.2	1.11	4.6	0.26	-51.4	0.77	385.1
Guizhou	29.82	28.9	2.78	-8.6	2.13	68.9	1.99	60.3	3.26	739.0
Yunnan	35.65	129.2	1.70	15.5	1.96	32.2	1.52	56.9	2.49	728.5
Xizang	1.07	235.3	0.004	23.1	0.26	95.7	0.13	888.7	0.46	15960.2

Table S2. Statistics comparing the pollution concentrations from the simulations with prior and posterior emissions against observations for July. CO unit: mg m^{-3}; others units: μg m^{-3}.

Species	Mean Obs.	Mean Sim.		BIAS		RMSE		CORR	
		CEP*	VEP*	CEP*	VEP*	CEP*	VEP*	CEP*	VEP*
CO	0.79	0.33	0.63	-0.46	-0.16	0.58	0.35	0.25	0.65
SO_2	12.9	15.6	9.6	2.7	-3.3	19.7	7.2	0.12	0.71
NO_2	20.0	23.0	16.5	3.0	-3.5	22.0	6.8	0.47	0.81
$PM_{2.5}$	29.2	21.9	23.3	-7.3	-6.0	21.1	13.9	0.51	0.76
PMC	53.6	27.6	42.3	-26.0	-11.3	42.3	30.9	0.38	0.61

* BIAS, mean bias; RMSE, root mean square error; CORR, correlation coefficient

References

Feng, S., Jiang, F., Jiang, Z., Wang, H., Cai, Z., and Zhang, L.: Impact of 3DVAR assimilation of surface PM2.5 observations on PM2.5 forecasts over China during wintertime, Atmospheric Environment, 187, 34-49, 2018.

Huang, X., Ding, A., Gao, J., Zheng, B., Zhou, D., Qi, X., Tang, R., Wang, J., Ren, C., Nie, W., Chi, X., Xu, Z., Chen, L., Li, Y., Che, F., Pang, N., Wang, H., Tong, D., Qin, W., Cheng, W., Liu, W., Fu, Q., Liu, B., Chai, F., Davis, S. J., Zhang, Q., and He, K.: Enhanced secondary pollution offset reduction of primary emissions during COVID-19 lockdown in China, National Science Review, doi: 10.1093/nsr/nwaa137, 2020. 2020.

Shi, X. and Brasseur, G. P.: The Response in Air Quality to the Reduction of Chinese Economic Activities During the COVID-19 Outbreak, 47, e2020GL088070, 2020.

Zheng, B., Zhang, Q., Geng, G., Chen, C., Shi, Q., Cui, M., Lei, Y., and He, K.: Changes in China's anthropogenic emissions and air quality during the COVID-19 pandemic in 2020, Earth Syst. Sci. Data, 13, 2895-2907, 2021.

Zhi, G., Zhang, Y., Sun, J., Cheng, M., Dang, H., Liu, S., Yang, J., Zhang, Y., Xue, Z., Li, S., and Meng, F.: Village energy survey reveals missing rural raw coal in northern China: Significance in science and policy, Environmental Pollution, 223, 705-712, 2017.